Supporting information

Synergistic catalysis of graphitic carbon nitride supported bimetallic sulfide nanostructures for efficient oxygen generation

Huixian Wang[a], Jinshen Ren[b], Aijian Wang[b,*], Qian Wang[a], Wei Zhao[a], Long Zhao[b]

[a] School of Energy & Power Engineering, Jiangsu University, Zhenjiang 212013, P.R. China

[b] School of Chemistry & Chemical Engineering, Jiangsu University, Zhenjiang 212013, P.R. China

Corresponding Author. Tel: +86-511-88791928. E-mail: wajujs@ujs.edu.cn

Experimental section

Characterization

X-ray diffraction (XRD) patterns of the as-prepared samples were performed on the XD-3 diffractometer with Cu Ka radiation in the 2θ range from $10°$ to $70°$. Transmission electron microscopy (TEM) was recorded on a JEM-2100 HR, JEOL system to investigate the morphology of the samples. The scanning electron microscopy (SEM) was carried out on a Model S4800, Hitachi, while the elemental spectrum including energy dispersive X-ray spectroscopy (EDS) was also recorded with the same experimental setup. The composition and chemical bond were determined by the X-ray photoelectron spectroscopy (XPS, a RBD upgraded PHI-5000C ESCA). Fourier transformed-infrared (FTIR) spectra were collected with a Bruker TENSOR 27FTIR spectrometer using KBr as pellets. Raman spectra were recorded on a micro-Raman spectrometer system with a laser beam of 532 nm at room temperature.
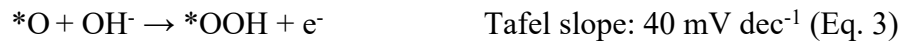
Electrochemical measurements

All electrochemical measurements including oxygen evolution reaction (OER) were performed with a CHI 614E electrochemical workstation (CH Instrument, China). The 1.0 M KOH solution was used as the electrolyte. The prepared samples decorated carbon fiber paper (CFP) was employed as the working electrode; The reference electrode is the mercury/mercury oxide electrode (MOE), and the counter electrode is the Pt gauze (1×1 cm^2). The preparation of working electrode is described as follows. The as-prepared samples (3 mg) was added into the mixed solution of Nafion solution (5 wt%, 40 μL),

CH$_3$CH$_2$OH (0.5 mL) and deionized water (0.5 mL). And then the obtained suspension was sonicated for 0.5 h to afford the homogeneous ink. Lastly, the obtained homogeneous ink (80 μL) was dropped onto the CFP, and then dried at room temperature and retained for use. The total geometric area of each sample is defined to be 0.5 cm^{-2} by Kapton tape. The mass loading amount is about 0.23 mg cm^{-2}. The electrochemical impedance spectroscopy (EIS) was recorded over the frequencies ranging from 0.01 Hz to 100 KHz in 1.0 M KOH. All potentials reported in this work were referenced to the reversible hydrogen electrode potential (RHE) based on the Nernst equation: $E_{RHE} = E_{MOE} + 0.0592pH + 0.098$. The OER data of the as-prepared samples were recorded by using the linear sweep voltammetry (LSV) in 1.0 M KOH solution. The overpotential was determined by the following equation: $\eta = E_{RHE} - 1.23$ V toward OER. The long-term stability of the samples was investigated with the chronoamperometry and chronopotentiometry method by using the same electrolyzer. To estimate the electrochemical surface areas (ECSA), the double-layer capacitance was determined by the cyclic voltammograms in the non-Faradaic potential region (0.1-0.2 V $vs.$ RHE) at different scan rates of 20, 40, 60, 80, and 100 mV/s, respectively. In a closed electrolytic cell, the generated oxygen was introduced into the gas chromatograph with a constant flow rate of argon to determine the Faraday efficiency of oxygen.

Tafel slope

The Tafel slopes were obtained with the fitted polarization data based on the Tafel equation ($\eta = b*logj + a$, where j represents the current density, η represents the overpotential, and b represents the Tafel slope). In the present case, the Tafel slope is used to evaluate the primary activities toward OER.

The OER mechanism generally accepted in alkaline electrolyte is the following path (Eqs. 1-4) [1]:

$$* + OH^- \rightarrow *OH + e^- \qquad \text{Tafel slope: 120 mV dec}^{-1} \text{ (Eq. 1)}$$
$$*OH + OH^- \rightarrow *O + H_2O + e^- \qquad \text{Tafel slope: 60 mV dec}^{-1} \text{ (Eq. 2)}$$
$$*O + OH^- \rightarrow *OOH + e^- \qquad \text{Tafel slope: 40 mV dec}^{-1} \text{ (Eq. 3)}$$
$$*OOH + OH^- \rightarrow * + O_2 + H_2O + e^- \qquad \text{Tafel slope: 15 mV dec}^{-1} \text{ (Eq. 4)}$$

Where * is an active site of the catalyst, *M represents an adsorbed intermediate on the catalyst surface.

Materials

Ammonium fluoride (NH_4F), potassium hydroxide (KOH), urea ($CO(NH_2)_2$), sodium sulfide (Na_2S), Nafion solution (5 wt%), Ammonium tetrathiomolybdate (($NH_4)_2MoS_4$), nickel chloride ($NiCl_2$) and melamine ($C_3H_6N_6$) were obtained from Sinopharm Chemical Reagent Co., Ltd. (China, Shanghai). All chemicals and reagents mentioned are of analytical grade and used as received without further treatment. The high-purity deionized water was used in whole experimental processes.

Preparation of $Ni_3S_2/MoS_2/ng\text{-}C_3N_4$ composite electrocatalysts

$Ni_3S_2/MoS_2/ng\text{-}C_3N_4$ composite electrocatalysts were prepared by a hydrothermal method and subsequently a thermal annealing approach. Typically, NH_4F (0.1 g), urea (0.4 g), Na_2S (0.15 g), ($NH_4)_2MoS_4$ (0.16 mg) and $NiCl_2$ (0.16 mg) were added into a mixed solution of deionized water (15 mL) and ethanol (15 mL), and ultrasonicated for 40 min to form a homogeneous dispersion. The mixed solution was poured into a 100 mL Teflon-lined autoclave, and then heated to 180 ^oC and kept for 12 h. The gray black solid was obtained by centrifugation, washed with ethanol and deionized water for several times, and freeze-dried overnight. To prepare $Ni_3S_2/MoS_2/g\text{-}C_3N_4$ composite electrocatalysts, a certain amount of $C_3H_6N_6$ was added into above prepared solid (50 mg), and then was calcined in a tube furnace at 750 ^oC for 2 h under a N_2 atmosphere. Finally, a gray product was obtained. To evaluate the influence of the loading content of $g\text{-}C_3N_4$ on the OER performance of $Ni_3S_2/MoS_2/ng\text{-}C_3N_4$, the amount of $C_3H_6N_6$ (as the precursor to $g\text{-}C_3N_4$) was varied (10, 20 and 30 mg); the corresponding samples were denoted as $Ni_3S_2/MoS_2/10g\text{-}C_3N_4$, $Ni_3S_2/MoS_2/20g\text{-}C_3N_4$ and $Ni_3S_2/MoS_2/30g\text{-}C_3N_4$, respectively. The Ni_3S_2, MoS_2 and Ni_3S_2/MoS_2 samples were also prepared as a reference with the similar experimental processes in the absence of $C_3H_6N_6$. For comparison purpose, the pristine $g\text{-}C_3N_4$ is also prepared by the thermal annealing approach.

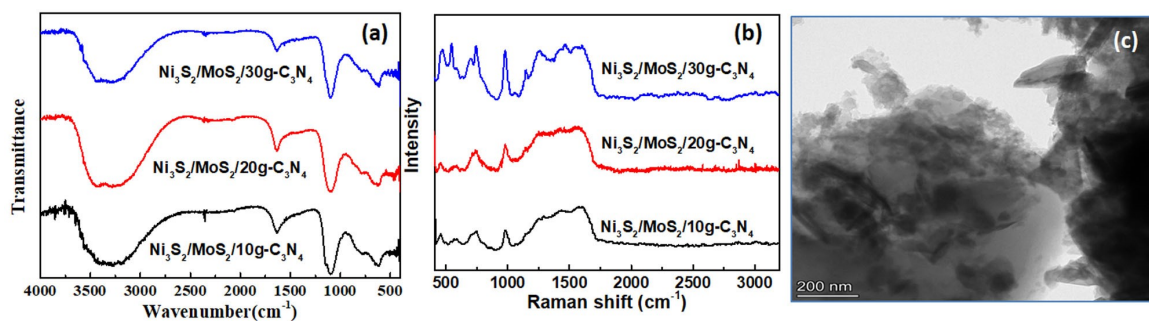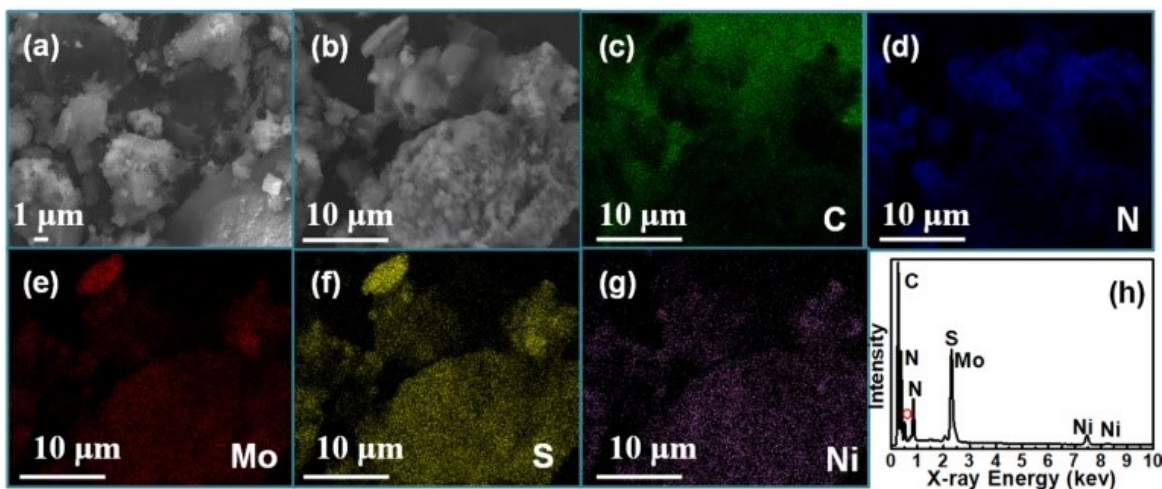Figure S1. (a) FTIR and (b) Raman spectra of the samples; (c) TEM image of $Ni_3S_2/MoS_2/20g-C_3N_4$.

Figure S2. (a-b) SEM images, (c-g) elemental mapping spectra and (h) EDS image of $Ni_3S_2/MoS_2/20g-C_3N_4$.
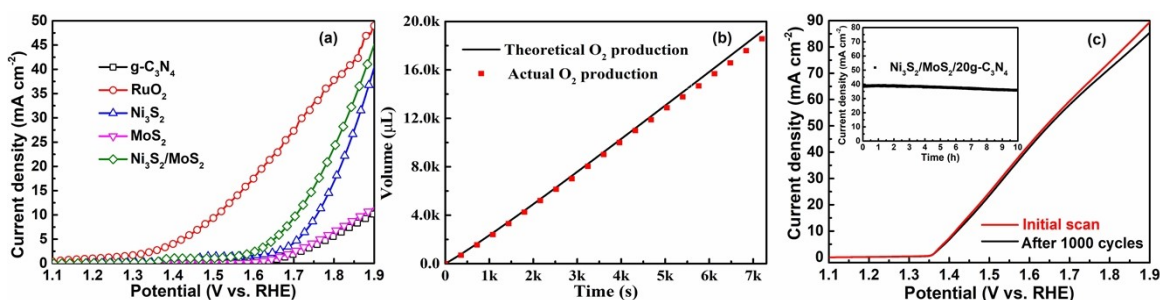

Figure S3. (a) OER polarization curves of the samples, (b) comparison of the theoretical and actual O_2 production and (c) OER LSV curves before and after 1000 cycles of CV scanning (Inset is the chronoamperometric data for $Ni_3S_2/MoS_2/20g-C_3N_4$).
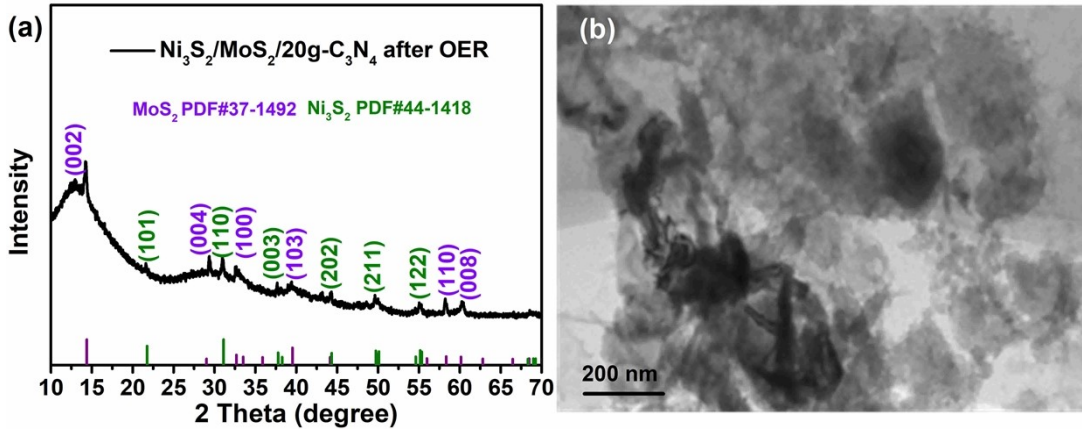
Figure S4. (a) XRD pattern and (b) TEM image of $Ni_3S_2/MoS_2/20g\text{-}C_3N_4$ after OER.
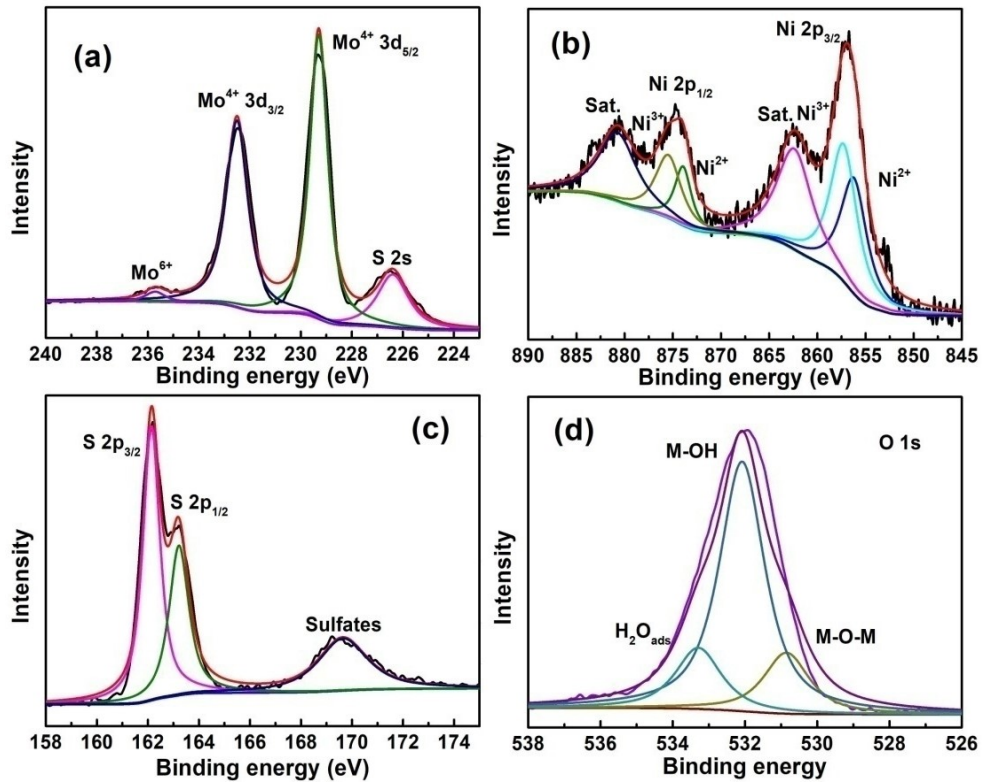

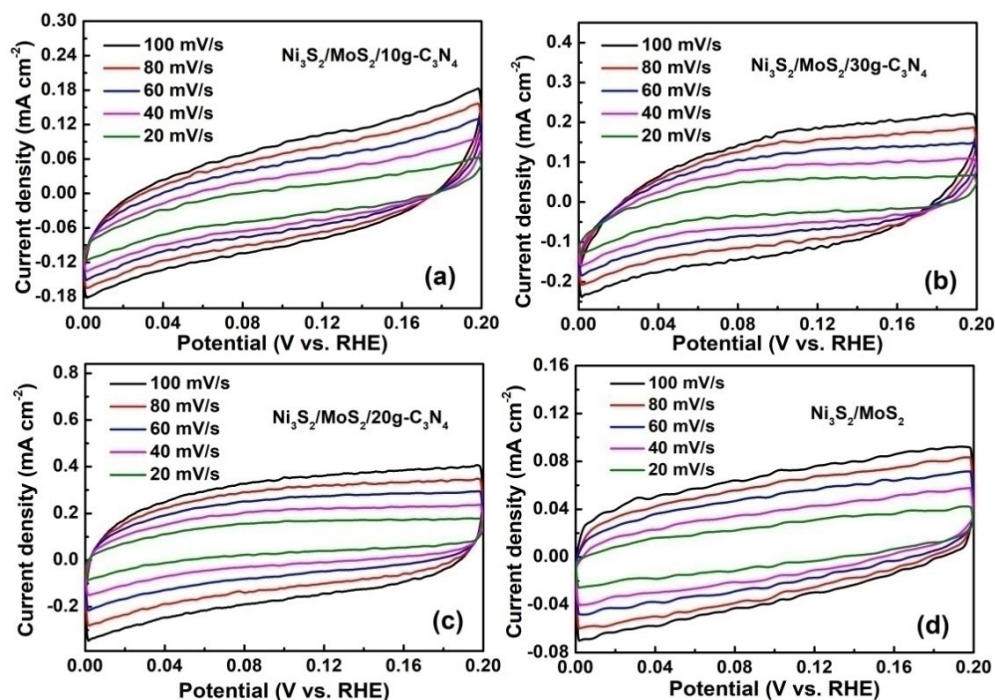Figure S5. XPS spectra of (a) Mo 3d, (b) Ni 2p, (c) S 2p and (d) O 1s for $Ni_3S_2/MoS_2/20g\text{-}C_3N_4$ after OER.

Figure S6. Electrochemical cyclic voltammograms of the samples at different scan rates.

Table S1. Comparison of the OER performance of $Ni_3S_2/MoS_2/20g-C_3N_4$ with other electrocatalytic systems.

Catalyst	η_{10} (mV)	References
$20\%CeO_2@CoS/MoS_2$	247	2
$CFP@MoS_2-70pp20$	273	3
$MoS_2/CoAl-LDH$	310	4
$Ni_3S_2@Ni_2P/MoS_2/NF$	175	5
$Co_3O_4-MoS_2$	298	6
$Ti_3C_2Tx@TiO_2/MoS_2$	270	7
$MoS_2@NiFe_2O_4$	290	8
$(MoS_2)_{0.125}Mo_2C$	280	9
$Co@MoS_2$	270	10
$MCNTs@CoS_x@MoS_2$	285	11
$NiSe_2@MoS_2$	267	12
$g-C_3N_4@carbon$ microflowers	450	13
$Co_3O_4/P-CN$	320	14
$Au/g-C_3N_4-AM1.5$	400	15

5.9wt% Ir/g-C$_3$N$_4$/NG	287	16
Ni(OH)$_2$/g-C$_3$N$_4$ composite	240	17
Co$_4$N@g-C$_3$N$_4$ nanotubes	285	18
NiCo$_2$S$_4$@g-C$_3$N$_4$-CNT	330	19
MoS$_2$ /Ni$_3$S$_2$	218	20
V-Ni$_3$S$_2$@CoFe-LDH/NF	190	21
Ni$_3$S$_2$/MoS$_2$ hollow spheres	303	22
MoS$_2$−Ni$_3$S$_2$-HNRs/NF	249	23
Ni$_3$S$_2$/Ni@CC	291	24
Ni-Fe-P-Ni$_3$S$_2$	219	25
Ni$_3$S$_2$/FeNi$_2$S$_4$	201	26
P-doped Ni$_3$S$_2$/NF	216	27
N-Ni$_3$S$_2$@NG	238	28
Fc-Ni$_9$S$_8$/Ni$_3$S$_2$-NC	222	29
Ni$_3$S$_2$@FeNi$_2$S$_4$@NF	235	30
FeS/Ni$_3$S$_2$	192	31
N-doped Ni$_3$S$_2$/CoS$_2$	245	32
AQS/S (A-AQS/S)	133	33
Co-Ni$_3$S$_2$	228	34
Fe-doped Ni$_3$S$_2$	267	35
Mo-Ni$_3$S$_2$	222	36
Carbon Layer Coated Ni$_3$S$_2$/MoS$_2$	350	37
Fe, Mn-Ni$_3$S$_2$	216	38
Ni$_2$P-Ni$_3$S$_2$	210	39
Ni$_3$S$_2$/NF	243	40
MoS$_2$/Co$_9$S$_8$/Ni$_3$S$_2$/Ni	166	41
Ni$_3$S$_2$@NiV-LDH	190	42
Co$_{0.9}$S$_{0.58}$P$_{0.42}$	266	43
Ni(OH)$_2$/MoS$_2$	360	44
CoSAs-MoS$_2$/TiN NRs	340.6	45
Co,Nb-MoS$_2$/TiO$_2$ HSs	260	46
O-MoS$_2$@Pt	244	47
Ni$_3$S$_2$/MoS$_2$	260	48

MoO$_2$@MoS$_2$@Co$_9$S$_8$	310	49
Co$_9$S$_8$@MoS$_2$/N-doped carbon	233	50
CoN/Ni$_3$N	247	51
Ni$_3$S$_2$/MoS$_2$/20g-C$_3$N$_4$	**183**	**This work**

Table S2. The fitting results of EIS spectra for the samples.

Samples	R$_{ct}$ (Ω)
Ni$_3$S$_2$/MoS$_2$/20g-C$_3$N$_4$	0.3
Ni$_3$S$_2$/MoS$_2$/30g-C$_3$N$_4$	1.1
Ni$_3$S$_2$/MoS$_2$/10g-C$_3$N$_4$	16.8
Ni$_3$S$_2$/MoS$_2$	34.1

References

1. K. Wan, J. Luo, C. Zhou, T. Zhang, J. Arbiol, X. Lu, B. W. Mao, X. Zhang, J. Fransaer, Hierarchical porous Ni$_3$S$_4$ with enriched high-valence Ni sites as a robust electrocatalyst for efficient oxygen evolution reaction, Adv. Funct. Mater. 29 (2019) 1900315.
2. W.H. Huang, X.M. Li, X.F. Yang, H.Y. Zhang, P.B. Liu, Y.M. Ma, X. Lu, CeO$_2$-embedded mesoporous CoS/MoS$_2$ as highly efficient and robust oxygen evolution electrocatalyst, Chem. Eng. J. 420 (2021) 127595.
3. Y. Huang, L. Liu, X. Liu, Modulated electrochemical oxygen evolution catalyzed by MoS$_2$ nanoflakes from atomic layer deposition, Nanotechnology 30 (2019) 095402.
4. M. Rong, F. Yang, C. Yu, S. Wang, H. Zhong, Z. Cao, MoS$_2$/CoAl-LDH heterostructure for enhanced efficient of oxygen evolution reaction, Colloid. Surf. A 607 (2020) 125419.
5. X. Yu, S. Xu, Z. Wang, S. Wang, J. Zhang, Q. Liu, Y. Luo, Y. Du, X. Sun, Q. Wu, Self-supported Ni$_3$S$_2$@Ni$_2$P/MoS$_2$ heterostructures on nickel foam for an outstanding oxygen evolution reaction and efficient overall water splitting, Dalton Trans. 50 (2021) 15094.
6. A.G. Abd-Elrahim, D.M. Chun, Nanosized Co$_3$O$_4$-MoS$_2$ heterostructure electrodes for improving the oxygen evolution reaction in an alkaline medium, J. Alloys Compd. 853 (2021) 156946.
7. X. Liu, D. Wang, Y. Du, X. Zhang, S. Ye, Construction of hierarchical Ti$_3$C$_2$Tx@TiO$_2$/MoS$_2$ covered manganese oxides for advanced oxygen evolution electrocatalysis, J. Mater. Sci. 56 (2021) 18174-18187.
8. M. Karpuraranjith, Y. Chen, B. Wang, J. Ramkumar, D. Yang, K. Srinivas, W. Wang, W. Zhang, R. Manigandan, Hierarchical ultrathin layered MoS$_2$@NiFe$_2$O$_4$ nanohybrids as a bifunctional catalyst for highly efficient oxygen evolution and organic pollutant degradation, J. Colloid Interf. Sci. 592 (2021) 385-396.
9. A.P. Tiwari, Y. Yoon, T.G. Novak, A. Azam, M. Lee, S.S. Lee, G. Lee, D.J.

Srolovitz, K.S. An, S. Jeon, Lattice strain formation through spin-coupled shells of MoS_2 on Mo_2C for bifunctional oxygen reduction and oxygen evolution reaction electrocatalysts, Adv. Mater. Interfaces 6 (2019) 1900948.

10. D. Xiong, Q. Zhang, W. Li, J. Li, X. Fu, M.F. Cerqueira, P. Alpuim, L. Liu, Atomic-layer-deposited ultrafine MoS_2 nanocrystals on cobalt foam for efficient and stable electrochemical oxygen evolution, Nanoscale 9 (2017) 2711-2717.

11. C. Wang, L. Zhang, G. Xu, L. Yang, J. Yang, Construction of unique ternary composite $MCNTs@CoS_x@MoS_2$ with three-dimensional lamellar heterostructure as high-performance bifunctional electrocatalysts for hydrogen evolution and oxygen evolution reactions, Chem. Eng. J. 417 (2021) 129270.

12. Y. Huang, J. Huang, K. Xu, R. Geng, Constructing $NiSe_2@MoS_2$ nano-heterostructures on a carbon fiber paper for electrocatalytic oxygen evolution, RSC Adv. 11 (2021) 26928-26936.

13. Z. Tong, D. Yang, X. Zhao, J. Shi, F. Ding, X. Zou, Z. Jiang, Bio-inspired synthesis of three-dimensional porous $g-C_3N_4@carbon$ microflowers with enhanced oxygen evolution reactivity, Chem. Eng. J. 337 (2018) 312-321.

14. M. Zhu, S. Yu, R. Ge, L. Feng, Y. Yu, Y. Li, W. Li, Cobalt oxide supported on phosphorus-doped $g-C_3N_4$ as an efficient electrocatalyst for oxygen evolution reaction, ACS Appl. Energy Mater. 2 (2019) 4718-4729.

15. H. Wang, T. Sun, L. Chang, P. Nie, X. Zhang, C. Zhao, X. Xue, The $g-C_3N_4$ nanosheets decorated by plasmonic Au nanoparticles: A heterogeneous electrocatalyst for oxygen evolution reaction enhanced by sunlight illumination, Eletrochim. Acta 303 (2019) 110-117.

16. B. Jiang, T. Wang, Y. Cheng, F. Liao, K. Wu, M. Shao, $Ir/g-C_3N_4$/nitrogen-doped graphene nanocomposites as bifunctional electrocatalysts for overall water splitting in acidic electrolytes, ACS Appl. Mater. Interfaces 10 (2018) 39161−39167.

17. T. Li, X. Ma, J. Wu, F. Chu, L. Qiao, Y. Song, M. Wu, J. Lin, L. Peng, Z. Chen, $Ni(OH)_2$ microspheres in situ self-grown on ultra-thin layered $g-C_3N_4$ as a heterojunction electrocatalyst for oxygen evolution reaction, Electrochim. Acta 400 (2021) 139473.

18. N. Wang, B. Hao, H. Chen, R. Zheng, B. Chen, S. Kuang, X. Chen, L. Cui, Highly dispersed Co_4N nanoparticles coated by $g-C_3N_4$ nanotube: An active bifunctional electrocatalyst for oxygen reduction and oxygen evolution reaction, Chem. Eng. J. 413 (2021) 127954.

19. X. Han, W. Zhang, X. Ma, C. Zhong, N. Zhao, W. Hu, Y. Deng, Identifying the activation of bimetallic sites in $NiCo_2S_4@g-C_3N_4$-CNT hybrid electrocatalysts for synergistic oxygen reduction and evolution, Adv. Mater. 31 (2019) 1808281.

20. J. Zhang, T. Wang, D. Pohl, B. Rellinghaus, R.H. Dong, S.H. Liu, X.D. Zhuang, X.L. Feng, Interface engineering of $MoS_2/Ni3S_2$ heterostructures for highly enhanced electrochemical overall-water-splitting activity, Angew. Chem. Int. Ed. 128 (2016) 6814-6819.

21. R. Tong, M. Xu, H. Huang, C. Wu, X. Luo, M. Cao, X. Li, S. Wang, H. Pan, 3D V-$Ni_3S_2@CoFe$-LDH core-shell electrocatalysts for efficient water oxidation, Int. J. Hydrogen Energy 46 (2021) 39636-39644.

22. S. Kim, K. Min, H. Kim, R. Yoo, S.F. Shim, D. Lim, S.H. Baeck, Bimetallic-metal organic framework-derived Ni_3S_2/MoS_2 hollow spheres as bifunctional

electrocatalyst for highly efficient and stable overall water splitting, Int. J. Hydrogen Energy 47 (2022) 8165-8176.

23. Y. Yang, K. Zhang, H. Lin, X. Li, H.C. Chan, L. Yang, Q. Gao, MoS_2−Ni_3S_2 heteronanorods as efficient and stable bifunctional electrocatalysts for overall water splitting, ACS Catal. 7 (2017) 2357-2366.

24. H. Qian, B. Wu, Z. Nie, T. Liu, P. Liu, H. He, J. Wu, Z. Chen, S. Chen, A flexible Ni_3S_2/Ni@CC electrode for high-performance battery-like supercapacitor and efficient oxygen evolution reaction, Chem. Eng. J. 420 (2021) 127646.

25. Z. Li, K. Wang, X. Tan, X. Liu, G. Wang, G. Xie, L. Jiang, Defect-enriched multistage skeleton morphology Ni-Fe-P-Ni_3S_2 heterogeneous catalyst on Ni foam for efficient overall water splitting, Chem. Eng. J. 424 (2021) 130390.

26. Y. Wu, Y. Li, M. Yuan, H. Hao, X. San, Z. Lv, L. Xu, B. Wei, Operando capturing of surface self-reconstruction of Ni_3S_2/$FeNi_2S_4$ hybrid nanosheet array for overall water splitting, Chem. Eng. J. 427 (2022) 131944.

27. Y. Yang, H. Mao, R. Ning, X. Zhao, X. Zheng, J. Sui, W. Cai, Ar plasma-assisted P-doped Ni_3S_2 with S vacancies for efficient electrocatalytic water splitting, Dalton Trans., 50 (2021) 2007-2013.

28. B. Li, Z. Li, Q. Pang, Controllable preparation of N-doped Ni_3S_2 nanocubes@N-doped graphene-like carbon layers for highly active electrocatalytic overall water splitting, Electrochim. Acta 399 (2021) 139408.

29. P. Thangasamy, S. Nam, S. Oh, H. Randriamahazaka, I. Oh, Boosting oxygen evolution reaction on metallocene-based transition metal sulfides integrated with N-doped carbon nanostructures, ChemSusChem 14 (2021) 5004-5020.

30. Y. Yang, H. Meng, C. Kong, S. Yan, W. Ma, H. Zhu, F. Ma, C. Wang, Z. Hu, Heterogeneous Ni_3S_2@$FeNi_2S_4$@NF nanosheet arrays directly used as high efficiency bifunctional electrocatalyst for water decomposition, J. Colloid Interf. Sci. 599 (2021) 300-312.

31. H. Li, S. Yang, W. Wei, M. Zhang, Z. Jiang, Z. Yan, J. Xie, Chrysanthemum-like FeS/Ni_3S_2 heterostructure nanoarray as a robust bifunctional electrocatalyst for overall water splitting, J. Colloid Interf. Sci. 608 (2022) 536-548.

32. Q. Kong, N. Fan, S. Chen, X. Wu, L. Liu, R. Lang, Z. Gao, H. Guan, C. Dong, G. Chen, Interface engineering of N-doped Ni_3S_2/CoS_2 heterostructures as efficient bifunctional catalysts for overall water splitting, J. Electroanalyt. Chem. 895 (2021) 115516.

33. Y. Chen, Z. Yu, R. Jiang, J. Huang, Y. Hou, J. Chen, Y. Zhang, H. Zhu, B. Wang, M. Wang, 3D-stretched film Ni_3S_2 nanosheet/macromolecule anthraquinone derivative polymers for electrocatalytic overall water splitting, Small 17 (2021) 2101003.

34. C. Jin, P. Zhai, Y. Wei, Q. Chen, X. Wang, W. Yang, J. Xiao, Q. He, Q. Liu, Y. Gong, $Ni(OH)_2$ templated synthesis of ultrathin Ni_3S_2 nanosheets as bifunctional electrocatalyst for overall water splitting, Small 17 (2021) 2102097.

35. M. Wang, L. Zhang, J. Pan, M. Huang, H. Zhu, A highly efficient Fe-doped Ni_3S_2 electrocatalyst for overall water splitting, Nano Res. 14 (2021) 4740-4747.

36. H. Chen, Z. Yu, R. Jiang, J. Huang, Y. Hou, Y. Zhang, H. Zhu, B. Wang, M. Wang, W. Tang, Sulfur defect rich Mo-Ni_3S_2 QDs assisted by O-C=O chemical bonding for an efficient lectrocatalytic overall water splitting, Nanoscale 13 (2013) 6644-6653.

37. C.P. Wang, L.J. Kong, H. Sun, M. Zhong, H.J. Cui, Y.H. Zhang, D.H. Wang, J. Zhu,

X.H. Bu, Carbon layer coated Ni_3S_2/MoS_2 nanohybrids as efficient bifunctional electrocatalysts for overall water splitting, ChemElectroChem 6 (2019) 5603-5609.

38. J. Duan, Z. Han, R. Zhang, J. Feng, L. Zhang, Q. Zhang, A. Wang, Iron, manganese co-doped Ni_3S_2 nanoflowers in situ assembled by ultrathin nanosheets as a robust electrocatalyst for oxygen evolution reaction, J. Colloid Interface Sci. 588 (2021) 248-256.

39. L. Zeng, K. Sun, X. Wang, Y. Liu, Y. Pan, Z. Liu, D. Cao, Y. Song, S. Liu, C. Liu, Three-dimensional-networked Ni_2P/Ni_3S_2 heteronanoflake arrays for highly enhanced electrochemical overall-water-splitting activity, Nano Energy 51 (2018) 26-36.

40. J. Zhang, Y. Li, T. Zhu, Y. Wang, J. Cui, J. Wu, H. Xu, X. Shu, Y. Qin, H. Zheng, P.M. Ajayan, Y. Zhang, Y. Wu, 3D coral-Like Ni_3S_2 on Ni foam as a bifunctional electrocatalyst for overall water splitting, ACS Appl. Mater. Interfaces 10 (2018) 31330-31339.

41. Y. Yang, H. Yao, Z. Yu, S.M. Islam, H. He, M. Yuan, Y. Yue, K. Xu, W. Hao, G. Sun, H. Li, S. Ma, P. Zapol, M.G. Kanatzidis, Hierarchical nanoassembly of MoS_2/Co_9S_8/Ni_3S_2/Ni as a highly efficient electrocatalyst for overall water splitting in a wide pH range, J. Am. Chem. Soc. 141 (2019) 10417-10430.

42. Q. Liu, J. Huang, Y. Zhao, L. Cao, K. Li, N. Zhang, D. Yang, L. Feng, L. Feng, Tuning the coupling interface of ultrathin Ni_3S_2@NiV-LDH heterogeneous nanosheet electrocatalysts for improved overall water splitting, Nanoscale 11 (2019) 8855-8863.

43. Z.F. Dai, H.B. Geng, J. Wang, Y.B. Luo, B. Li, Y. Zong, J. Yang, Y.Y. Guo, Y. Zheng, X. Wang, Q.Y. Yan, Hexagonal-phase cobalt monophosphosulfide for highly efficient overall water splitting, ACS Nano 11 (2017) 11031-11040.

44. Z. He, Q. Liu, Y. Zhu, T. Tan, L. Cao, S. Zhao, Y. Chen, Defect-mediated adsorption of metal ions for constructing Ni hydroxide/MoS_2 heterostructures as high-performance water-splitting electrocatalysts, ACS Appl. Energy Mater. 3 (2020) 7039−7047

45. T.L.L. Doan, D.C. Nguyen, S. Prabhakaran, D.H. Kim, D.T. Tran, N.H. Kim, J.H. Lee, Single-atom Co-decorated MoS_2 nanosheets assembled on metal nitride nanorod arrays as an efficient bifunctional electrocatalyst for pH-universal water splitting, Adv. Funct. Mater. 2021, 2100233.

46. D.C. Nguyen, T.L.L. Doan, S. Prabhakaran, D.T. Tran, D.H. Kim, J.H. Lee, N.H. Kim, Hierarchical Co and Nb dual-doped MoS_2 nanosheets shelled micro-TiO_2 hollow spheres as effective multifunctional electrocatalysts for HER, OER, and ORR, Nano Energy 82 (2021) 105750.

47. F. Gong, S. Ye, M. Liu, J. Zhang, L. Gong, G. Zeng, E. Meng, P. Su, K. Xie, Y. Zhang, J. Liu, Boosting electrochemical oxygen evolution over yolk-shell structured O–MoS_2 nanoreactors with sulfur vacancy and decorated Pt nanoparticle, Nano Energy 78 (2020) 105284.

48. C. Wang, X. Shao, J. Pan, J. Hu, X. Xu, Redox bifunctional activities with optical gain of Ni_3S_2 nanosheets edged with MoS_2 for overall water splitting, Appl. Catal. B: Environ. 268 (2020) 118435.

49. Y. Li, C. Wang, M. Cui, J. Xiong, L. Mi, S. Chen, Heterostructured MoO_2@MoS_2@Co_9S_8 nanorods as high efficiency bifunctional electrocatalyst for

overall water splitting, Appl. Surf. Sci. 543 (2021) 148804.

50. M. Kim, H. Seok, N.C.S. Selvam, J. Cho, G.H. Choi, M.G. Nam, S. Kang, T. Kim, P.J. Yoo, Kirkendall effect induced bifunctional hybrid electrocatalyst (Co_9S_8@MoS_2/N-doped hollow carbon) for high performance overall water splitting, J. Powder Sources 493 (2021) 229688.

51. C. Ray, S.C. Lee, B. Jin, A. Kundu, J.H. Park, S.C. Jun, Conceptual design of three-dimensional CoN/Ni_3N-coupled nanograsses integrated on N-doped carbon to serve as efficient and robust water splitting electrocatalysts, J. Mater. Chem. A 6 (2018) 4466-4476.